

## Phonon mode softening and elastic properties of hafnium under pressure

Dmitry Novoselov,<sup>1,2,\*</sup> V. I. Anisimov,<sup>1,2</sup> and Yu. S. Ponosov<sup>1,2</sup>

<sup>1</sup>*M. N. Mikheev Institute of Metal Physics, Ural Branch of the Russian Academy of Sciences, 18 S. Kovalevskaya Street, Yekaterinburg 620137, Russia*

<sup>2</sup>*Department of Theoretical Physics and Applied Mathematics, Ural Federal University, 19 Mira Street, Yekaterinburg 620002, Russia*



(Received 21 February 2018; revised manuscript received 27 April 2018; published 30 May 2018)

The effect of pressure on the zone-center optical phonon modes and the elastic properties of hafnium have been studied employing both experimental (Raman scattering) and theoretical (density-functional theory) approaches. An anomaly dependence of the phonon frequency of the  $E_{2g}$  mode was found in the pressure range from 0 to 67 GPa. The calculated electronic structure of hafnium shows significant changes under pressure, which have a pronounced spatial anisotropy similar to the anisotropy of the observed phonon properties. The dependencies of the elastic properties on pressure, including the components of the elasticity tensor, bulk and shear modulus, Poisson ratio, and universal anisotropy index, obtained from the calculations have characteristic features indicating the occurrence of a structural phase transition.

DOI: [10.1103/PhysRevB.97.184108](https://doi.org/10.1103/PhysRevB.97.184108)

### I. INTRODUCTION

Transition metals in group IV (Ti, Zr, Hf) possess a hexagonal-close-packed structure (hcp- $\alpha$ ) at atmospheric pressure. When the pressure increases, they all undergo successive structural transitions, initially to the  $\omega$  phase with a simple hexagonal lattice with three atoms per unit cell and then to the cubic phase  $\beta$  with a bcc lattice. The crystal structure of hafnium under pressure was investigated using x-ray diffraction in [1], where it was reported that the transition to the  $\omega$  phase began at a pressure of 45.8 GPa and was completed at 58.3 GPa. The reverse transition from the  $\omega$  phase had a significant hysteresis, starting at 30 GPa and ending at 19.3 GPa. Subsequent x-ray investigation of hafnium at high pressures [2] did not reveal a transition to the  $\omega$  phase at room temperature in the pressure region up to 51 GPa. A mixture of  $\alpha$  and  $\omega$  phases was observed only with an increase in temperature up to 770 K at 45 GPa. The authors explained this discrepancy as the effects of nonhydrostaticity in experiment [1], which can decrease the temperature of the martensitic transition. Another x-ray study [3] at room temperature confirmed the existence of a sequence of the transformations  $\alpha \rightarrow \omega \rightarrow \beta$  in pure Hf. In [3] the  $\alpha \rightarrow \omega$  transition with a wide hysteresis began above the pressure  $P = 50.6$  GPa, and the  $\omega \rightarrow \beta$  transition occurred above 65 GPa. It has been shown that the use of different pressure-transmitting media results in small shifts in the transition pressures  $\alpha \rightarrow \omega$ , but the transition itself can be suppressed when the impurity concentration in the sample increases to 7.5%. In spite of the fact that some *ab initio* calculations of transition pressures have been carried out [4–10], the mechanism of structural instability of hafnium has been studied insufficiently both experimentally and theoretically. A recent experimental and theoretical study of the elastic properties of hafnium [10] showed the presence of

softening of shear moduli with an increase in pressure above 10 GPa, which could indicate the precursors of the  $\alpha \rightarrow \omega$  transition.

Raman spectroscopy can provide information not only about the structural state of a substance under pressure but also about the effect of changes in interatomic distances on the vibrational and electronic spectrum. Thus, the Raman studies of titanium and zirconium [11,12] revealed an anomalous behavior of the frequency of the  $E_{2g}$  phonon, which is softened in the  $\alpha$  phase under pressure. The relationship between the  $E_{2g}$  phonon frequency and the elastic modulus  $C_{44}$  suggested a decrease in the latter under pressure which was confirmed by subsequent ultrasonic measurements [13]. For hafnium, Raman measurements, as well as calculations of the phonon spectrum, have not yet been reported.

Despite the substantial interest [2,3,8–10] in this system from the scientific community, to date, there is a lack of unambiguous insight on the relationship between phonon properties and structural stability at high pressures in hafnium. In our work, the evolution of the phonon spectrum of hafnium in the pressure region from 0 to 67 GPa at room temperature is investigated by Raman spectroscopy. For the analysis and interpretation of experimental data, first-principles density-functional theory (DFT) calculations of phonon frequencies and elastic properties at different pressures are performed.

### II. METHODS

#### A. Experiment

Samples for measurements were cut from a hafnium single crystal with a purity of 99.8% with a residual resistivity ratio of  $\rho_{300K}/\rho_{4.2K} = 27$ . Thin (20- $\mu\text{m}$ ) plates with transverse dimensions up to 100  $\mu\text{m}$  were placed in the center of the flat culets (300  $\mu\text{m}$  in diameter) of diamond anvils. Because of the extremely low Raman intensity of the hafnium spectrum, the experiment was carried out without the use of a pressure-transmitting medium: the sample was compressed between

\*novoselov@imp.uran.ru

the anvil and the gasket. To further reduce the influence of additional sources of scattered light, we also used diamonds with the lowest level of luminescence that served as a pressure sensor. The pressure in the cell was determined from the shift of the high-frequency edge of the  $T_{2g}$  phonon diamond line in the sample region under study. Preliminary calibration of the dependence of the diamond-line frequency on the pressure in the anvils was carried out using the ruby luminescence method: the result practically coincided with the data of [14]. Two runs were performed. In the first, a gasket was made of steel, and the highest pressure was 50 GPa. In the second run, the pressure reached 67 GPa, and the use of a rhenium gasket provided an additional possibility of controlling the pressure [15]. The spectra were excited by lines of solid-state (532-nm) and helium-neon (633-nm) lasers focused (50 objective) on a spot 5–10  $\mu\text{m}$  in diameter. The scattered light was recorded in backscattering geometry using a Renishaw RM1000 spectrometer equipped with edge filters to exclude low-frequency Rayleigh scattering with a cutoff  $\approx 40\text{ cm}^{-1}$  and a cooled multichannel CCD detector.

### B. Calculations

Crystal structure data for Hf at different values of pressure were taken from Ref. [3], and one set has been used as the initial data for *ab initio* electronic structure calculations based on the generalized gradient approximation (GGA) of the DFT implemented in the VASP package [16–18]. In all the calculations the valence configuration is  $5p6s5d$  with four valence electrons. The frozen-phonon and linear response methods were used to evaluate the optical phonon mode frequencies at the  $\Gamma$  point of the Brillouin zone. The plane-wave energy cutoff was set to 450 eV, and we have used a  $\Gamma$ -centered  $12 \times 12 \times 12$   $k$ -point mesh for pressure values from 0 to 65 GPa. Self-consistent convergence of the energy was set to  $10^{-8}$  eV/cell, and the force-convergence criterion was  $10^{-7}$  eV/Å. We have solved the third-order Birch-Murnaghan equation of states [19] in order to receive an equilibrium volume of the cell  $V_0$ . The obtained value of  $V_0$  is  $22.49\text{ \AA}^3$ , which is close to the experimental equilibrium volume of  $22.41\text{ \AA}^3$ .

### III. RESULTS AND DISCUSSION

In the hcp phase of Hf, there are three optical phonon modes:  $B_{1g}$  and doubly degenerate  $E_{2g}$  modes. The first one corresponds to the atomic displacements of the Hf ions along the  $z$  direction. However, the  $E_{2g}$  phonon mode is associated with vibrational motion in the  $xy$  plane. According to the selection rules for hcp crystals in a Raman spectrum of the first order, one line, the  $E_{2g}$  optical phonon at the  $\Gamma$  point of the Brillouin zone, should be observed. In the spectra of hafnium at  $P = 0$  GPa (Fig. 1) a very narrow (about 2–3  $\text{cm}^{-1}$ ) peak at a frequency of  $85 \pm 1.5\text{ cm}^{-1}$  is recorded, whose energy is close to the value of the energy of the TO [0001] mode at  $\Gamma$  obtained in the neutron experiment,  $90 \pm 5.3\text{ cm}^{-1}$  [20].

In addition to this peak, broad lines at frequencies of 145 and 230–290  $\text{cm}^{-1}$  were found in the spectra. They are observed only for a parallel orientation of the polarization of the incident and scattered light ( $A_{1g}$  symmetry), which agrees with the selection rules for the two-phonon spectra activity in

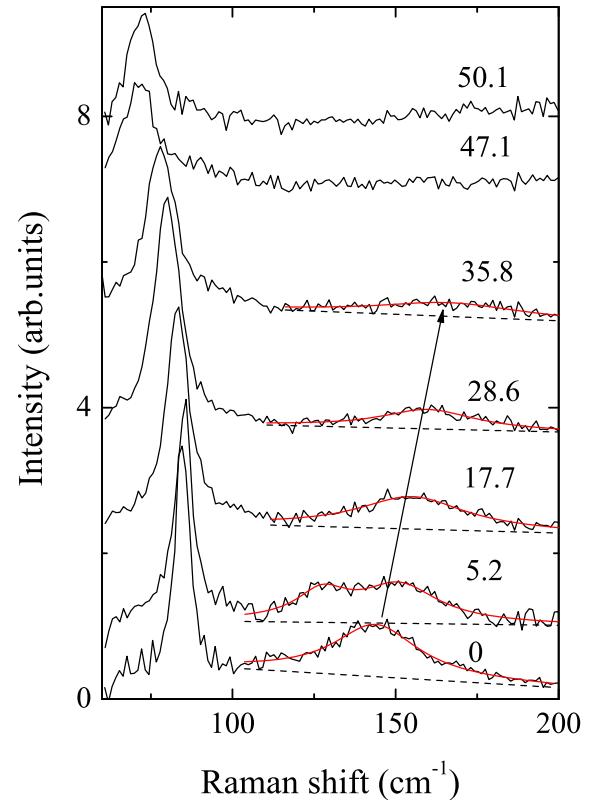


FIG. 1. Raman spectra of Hf measured in the first run using a 633-nm excitation wavelength. Peaks in second-order spectra are fitted with Lorentzians (solid lines), and backgrounds are shown with dashed lines.

hcp crystal. A comparison with the phonon dispersion from the neutron experiment [20] suggests that the feature near 145  $\text{cm}^{-1}$  is definitely associated with overtone scattering from transverse acoustic phonons at the  $M$  and  $A$  points of the Brillouin zone, while in the 235–290  $\text{cm}^{-1}$  region there are overtone excitations from several rather flat longitudinal and transverse branches near the  $M$  point. A rather large intensity of two-phonon scattering makes it possible to obtain information on the density of phonon states in hafnium from the Raman experiment. The spectra obtained under pressure in the first run (Fig. 1) show a slight increase in the  $E_{2g}$  mode frequency with an increase in pressure up to 10–15 GPa. With a further increase in pressure, an anomalous softening of the  $E_{2g}$  mode frequency is observed, while the energy of the broad feature at 145  $\text{cm}^{-1}$  is increased by 15% with the growth of  $P$  up to 35 GPa (Fig. 1).

At higher pressures, the intensity of this feature is lower than the observation limit. The high-frequency peak at 230–290  $\text{cm}^{-1}$  was not observed in measurements in the cell. The dependence of the  $E_{2g}$  mode frequency vs pressure from the first run is shown in Fig. 2. Its energy drops by  $\sim 17\%$  to 50 GPa. Such a softening of the mode was previously observed in the  $\alpha$  phase of zirconium [11] and was supposed to be due to changes in the electronic structure under pressure. Despite a significant decrease in the intensity of the  $E_{2g}$  mode to 50 GPa in the first run, no Raman-active  $E_{2g}$  phonon of the  $\omega$  phase was observed in the spectra. On pressure release, we did not

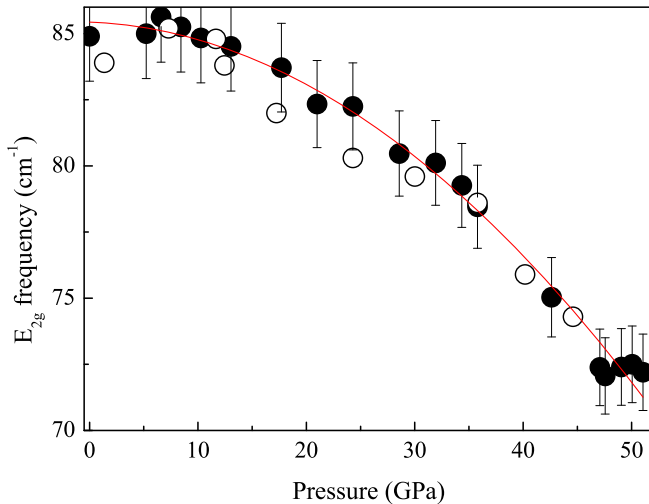


FIG. 2.  $E_{2g}$  phonon mode frequency of Hf vs pressure from the first run depicted by solid circles (with an increase in pressure), open circles (with a decrease in pressure), and the red line (guide to the eye).

observe hysteresis in the behavior of the phonon frequency (see Fig. 2).

Raman spectra of Hf measured in the second run up to 67 GPa are shown in Fig. 3. The pressure dependence of the  $E_{2g}$  frequency in the second run (see Figs. 3 and 4) coincides with the first-run data in the region up to 50 GPa. With a further

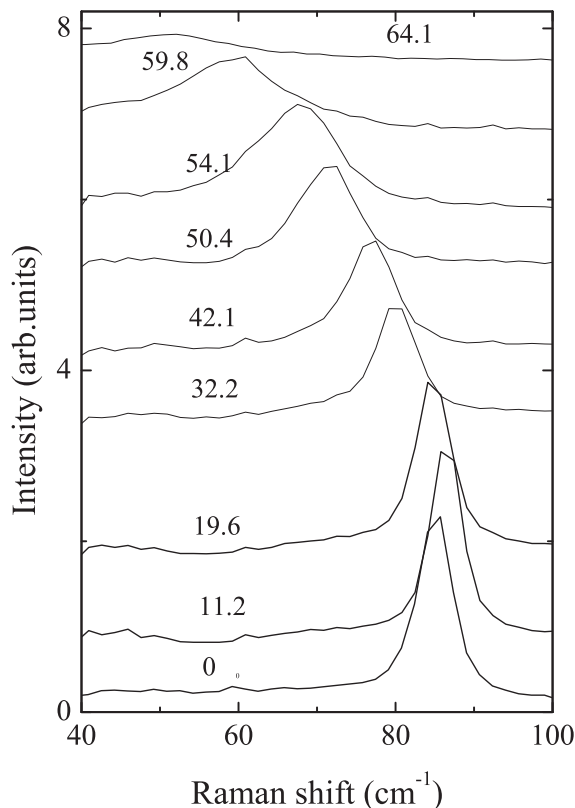


FIG. 3. Raman spectra of Hf at different pressures measured in the second run using a 532-nm excitation wavelength.

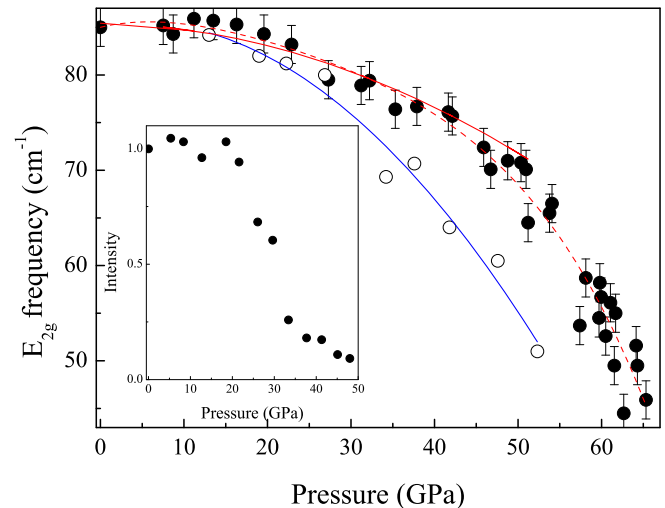


FIG. 4.  $E_{2g}$  phonon mode frequency of Hf vs pressure from the second run depicted by solid circles (with an increase in pressure) and the red dashed line (guide to the eye) and open circles (with a decrease in pressure) and the blue solid line. The red solid line corresponds to the first-run data with increasing pressure, and it is the same as in Fig. 2, which confirms the first-run results. The dependence of intensity under pressure release is shown in the inset.

increase in pressure, the frequency and intensity of the  $E_{2g}$  mode decrease significantly. The highest pressure at which this line was observed was 64 GPa. With an increase in pressure above 50 GPa, the reflection of the investigated region of the sample in the microscope changed its intensity and became shiny at a pressure of 65 GPa. At this pressure, we could not observe the phonon line, which suggests the achievement of transition pressure. On pressure release, the line appeared again at a pressure of 52 GPa, and its frequency showed a significant hysteresis, recovering at pressures of  $<20$  GPa (Fig. 4). We also observed that the sample changed appearance from shiny to black in reflected light on pressure release to 50 GPa. We believe that the sharp drop in the frequency of the  $E_{2g}$  mode above 50 GPa is associated with the onset of the transition to the  $\omega$  phase (as in Ref. [3]). However, in our measurements, it was not possible to observe the Raman-active  $E_{2g}$  phonon of the hexagonal high-pressure phase either on loading or when unloading the sample. Such a line was clearly observed in the Raman spectra of the  $\omega$  phase of titanium and zirconium [11,12]. The reason for that may be its weak intensity or its low frequency, which is unattainable for our spectrometer ( $<45$   $\text{cm}^{-1}$ ). The frequency hysteresis of the  $E_{2g}$  mode in the 20–50 GPa range (Fig. 4), which was not observed in the first experiment up to 50 GPa (Fig. 2), indicates the appearance of the phase in the second run. In addition, the intensity of the phonon line increased significantly on pressure release in the region from 40 to 20 GPa (inset in Fig. 4), which agrees with the data of [3] and perhaps indicates an increase in the amount of the alpha phase due to a corresponding decrease in the amount of the omega phase. These facts argue that, in spite of the absence of the  $\omega$  phase line in our spectra, the  $\alpha$  and  $\omega$  phases coexist in the region of 50–64 GPa on increasing pressure and in the region of 52–20 GPa on pressure release. The disappearance of the  $\alpha$  phase line at the highest pressure

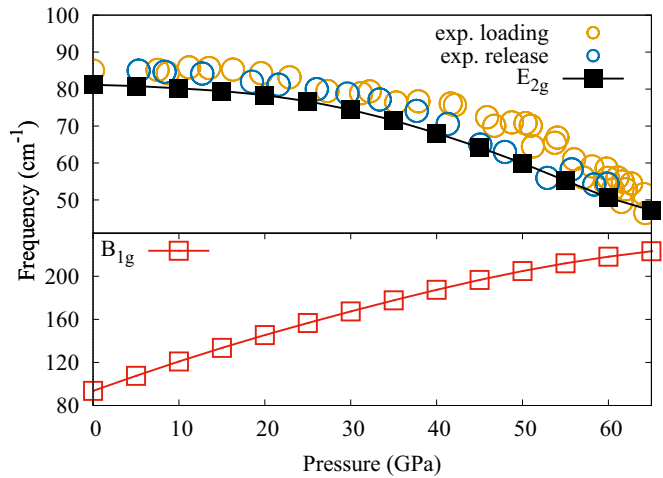


FIG. 5. Calculated frequencies of  $E_{2g}$  (black curve with solid squares in the top panel) and  $B_{1g}$  (red curve with open squares in the bottom panel) optical phonon modes at the  $\Gamma$  point; the experimental data indicated by blue and orange open circles correspond to a decrease and increase in pressure, respectively.

possibly implies a direct transition of the  $\alpha$  phase to the  $\beta$  phase [3].

Although the Raman experiment probes only the  $\Gamma = 0$  phonon, it is obvious that at least the transverse optical phonons with  $q = 1/6$  [010] in hafnium will be significantly softened under pressure. A significant decrease of the elastic modulus  $C_{44}$  (coupled with the  $E_{2g}$  phonon frequency) indicates the involvement of acoustic phonons with the same wave vector. These observations support the transformation mechanism proposed in [21].

To clarify the relationship of the anomalous behavior of the phonon mode with the electronic degrees of freedom of the system under study, the calculations in the framework of the density functional theory were carried out for  $\alpha$ -Hf crystal structures at different pressures. During the GGA calculations, the values of the phonon mode frequencies at the  $\Gamma$  point were obtained by the frozen-phonon method in the pressure range from 0 to 65 GPa. Our calculations confirmed the main results obtained in the experiment (see Fig. 5). As we can see from the top panel of Fig. 5, the frequency of the  $E_{2g}$  mode is softening, which is counterintuitive behavior during compression. At the same time, the calculated frequency of the  $B_{1g}$  phonon mode increases under pressure (bottom panel in Fig. 5). The small difference between the calculated and experimental data may be because nonhydrostatic pressure is applied in the experiment. Also, it is possible [8] that taking the spin-orbit interaction into account in the calculations could slightly improve the quantitative agreement with experiment.

To determine the influence of pressure on the electronic structure of the  $\alpha$  phase of hafnium, the total and partial densities of states were obtained. The densities of hafnium  $5p6s$  and  $5d$  states are presented in Fig. 6 for two pressure values, 0 and 50 GPa. The general shape and positions of the peaks are in good agreement with previously published data [5,8]. There are two competing effects which influence the occupation of the  $d$  level near the Fermi energy with a change in pressure. The first is connected to the effect of

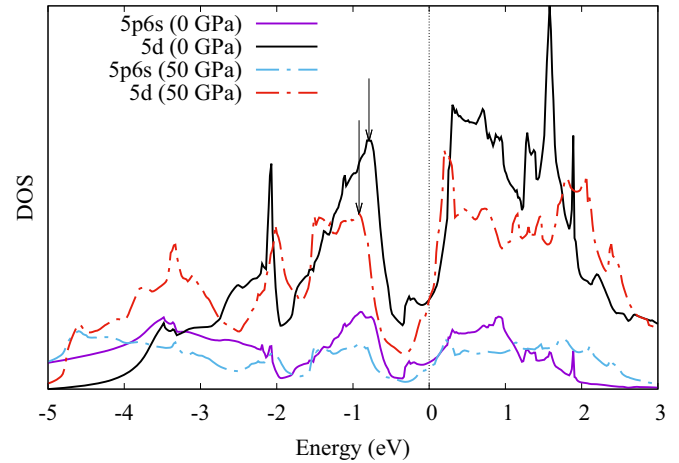


FIG. 6. The density of  $5p6s$  (violet and blue) and  $5d$  Hf (black and red) states at 0 and 50 GPa pressure is depicted by solid and dash-dotted curves, respectively. The Fermi level is placed at zero energy and denoted by the dashed vertical line. The vertical arrows indicate the centers of the  $d$  peak near the Fermi level in the valence band.

broadening of the relatively narrow peak under compression, which leads to a decrease of the  $d$ -state occupation due to the increase in the area under the curve above the Fermi level. The second one is due to the shift of the peak downward in energy, which leads to an increase in the occupation of the corresponding states. In Fig. 6 the vertical arrows indicate the centers of the peaks under the Fermi level. As we can see, there is a shift of the peak to lower energy when pressure is applied. The value of the shift is about 0.13 eV. Along with this effect, the broadening of the bands below  $-2$  eV towards lower energies is observed. In addition, it can be observed that the density of  $5d$  states at the Fermi level remains unchanged under compression as if the band were attached to the zero energy. Such a redistribution of the density of states leads to an increase in the occupation of the  $5d$  level. Figure 6 also shows the density of  $sp$  Hf states. The position and the structure of the peaks on the curves quite clearly repeat the ones in the  $d$  band, which confirms the presence of a strong hybridization between corresponding states. The growth of the number of  $d$  electrons is associated with the rise in the hybridization between  $d$  and  $sp$  levels of neighboring atoms with increasing pressure due to the decreasing of the interatomic distances, which leads to reducing the occupation of the  $sp$  states. In the  $\alpha$  phase the distances between the nearest-neighboring hafnium atoms are different for atoms in the  $ab$  plane and atoms in neighboring planes. With increasing pressure, these distances and also the difference between them decrease up to a pressure of 70 GPa, at which the corresponding lengths coincide [3]. The number of  $5d$  electrons changes from 2.11 at 0 GPa pressure to 2.30 at 50 GPa, which agrees well with the previously published data [8]. For a more detailed analysis of the change in the density of states with increasing pressure the partial density of  $5d$  Hf states was constructed and is shown in Fig. 7 in comparison with  $6s$  and  $5p$  Hf states. Figure 7 shows clearly that  $6s$  states have the largest hybridization, with  $5d$  states with  $xy$  and  $yz$  symmetry having the lowest density of states.

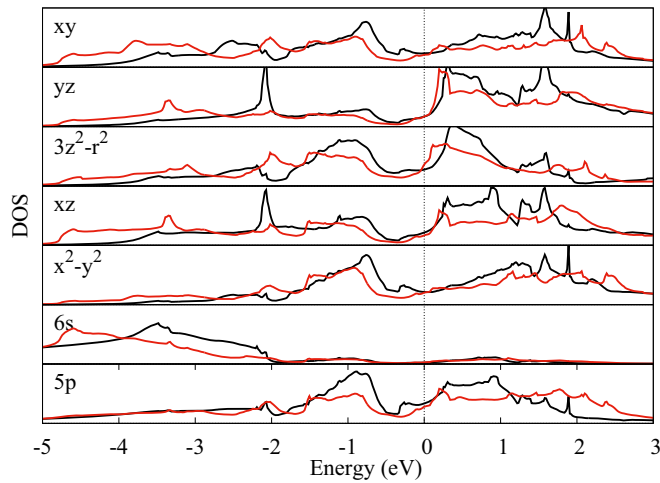


FIG. 7. The density of states for  $5d$ ,  $6s$ , and  $5p$  levels at 0 GPa (black curve) and 50 GPa (red curve) pressures. The Fermi level corresponds to zero energy.

The  $5p$  states hybridize predominantly with  $x^2-y^2$ ,  $xy$ , and  $3z^2-r^2$  states in the region from  $-2.5$  eV to the Fermi level, as indicated by a pronounced peak near  $-0.8$  eV. From Fig. 7, it follows that the occupation of  $6s$  states remains unchanged, whereas the area under the  $5p$  curve below  $E_F$  is decreased when pressure is applied. As we can see from Fig. 7, the orbitals with  $x^2-y^2$  and  $xy$  symmetry undergo the most noticeable shift of that relatively narrow peak edge, which may indicate their dominant contribution to the redistribution of the density of states near the Fermi level as a result of the growth of the  $pd$  hybridization. The average value of the peak edge shift is about 0.25 eV. At the same time, the edge of the peak under the Fermi level on the density of states of the  $3z^2-r^2$  orbital has no such shift with increasing pressure. Thus, the redistribution of the density of states, which has the largest contribution near the Fermi level, has a pronounced spatial anisotropy. These observations are consistent with the results of an analysis of the change in the charge density at external pressure. Figure 8(a) presents the schematic view of the crystal structure of  $\alpha$ -Hf and the isosurface of the charge density difference between 45- and 65-GPa pressure, and the spatial shapes of  $5d$  atomic orbital combinations are shown in Fig. 8(b). The important thing here is the shape of the isosurface of the positive charge density difference, which repeats the shape of the square moduli sum of the wave functions of general  $5d$  states with  $x^2+y^2$  and  $xy$  symmetries [left shape in Fig. 8(b)] to a greater degree than those of  $3z^2+r^2$  or  $xz$  and  $yz$  symmetries [middle and right shapes in Fig. 8(b)]. The negative difference of the charge density has a spherical-like shape which is probably due to a decrease in the occupation of the  $5p$  Hf states. This visually illustrates the effect of redistribution of the density of states, which is connected to the spatial orientation of the partially filled  $d$  and  $sp$  orbitals and to the increasing of the overlap area between them under pressure. In this way, during the pressure increase, it is advantageous to redistribute the charge density to the  $xy$  plane but not in the  $z$  direction.

To understand the mechanical instability of the  $\alpha$ -Hf structure and possible causes of the  $\alpha \rightarrow \omega$  phase transition the

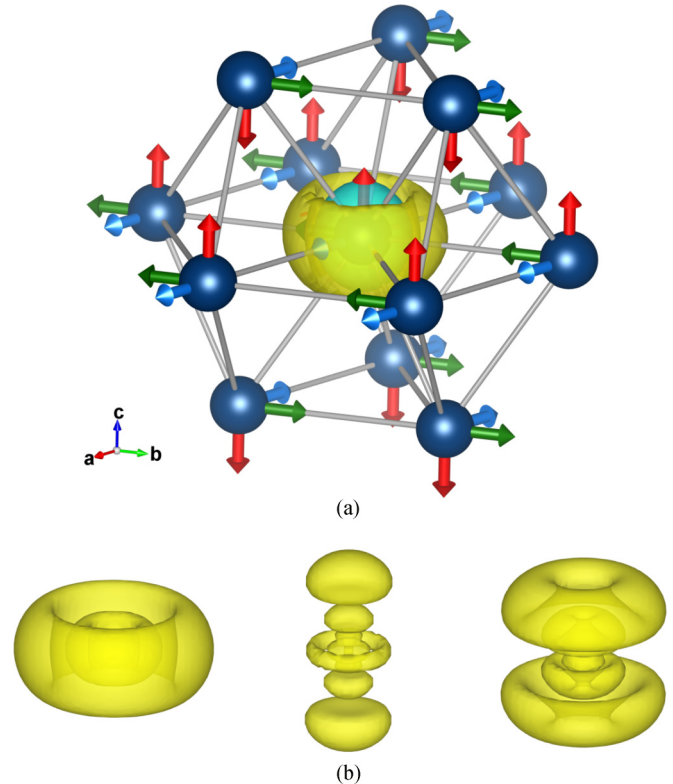


FIG. 8. (a) The crystal structure of  $\alpha$ -Hf and the isosurface of the charge density difference (shown only for the central atom) under compression. The navy blue spheres denote the hafnium atoms. The yellow and blue regions of the isosurface indicate positive and negative differences in charge densities, respectively. The arrows denote the directions of the atomic displacements corresponding to the phonon vibrational modes: green and blue show doubly degenerate  $E_{2g}$ , and red shows  $B_{1g}$ . (b) The spatial shape of the atomic  $5d$  orbitals obtained as the squared moduli of the  $5d$  wave functions: from left to right, sum of  $x^2 + y^2$  and  $xy$ ,  $3z^2 + r^2$ , and sum of  $xz$  and  $yz$ .

change in the elastic and mechanical properties under pressure were investigated. The components of the elasticity tensor at various values of the external pressure were determined in the course of the calculations. Figure 9 shows the dependencies of the values of the nonzero components of the elasticity tensor on pressure, and the values are in good agreement with those presented in the literature [10].

Figure 10 shows the results of calculating of the elastic constant  $C_{44}$  obtained both during the DFT calculations and from the experimental data by using a simple model [22,23] of the lattice dynamics of hcp metals implementing the relationship between the value of the elastic constant  $C_{44}$  and the phonon frequency of the  $E_{2g}$  mode in the following form:

$$C_{44} = \frac{mc}{4\sqrt{3}a^2} \omega_{E_{2g}}^2, \quad (1)$$

where  $a$  and  $c$  are the lattice constants,  $m$  is the atomic mass, and  $\omega_{E_{2g}}$  is the frequency of the  $E_{2g}$  mode. Both the experiment and the calculation show a dramatic decrease ( $\sim 2$  times) in the  $C_{44}$  elastic constant value under compression (see Fig. 10). The value of  $C_{44}$  at  $P = 0$  GPa, obtained from the Raman

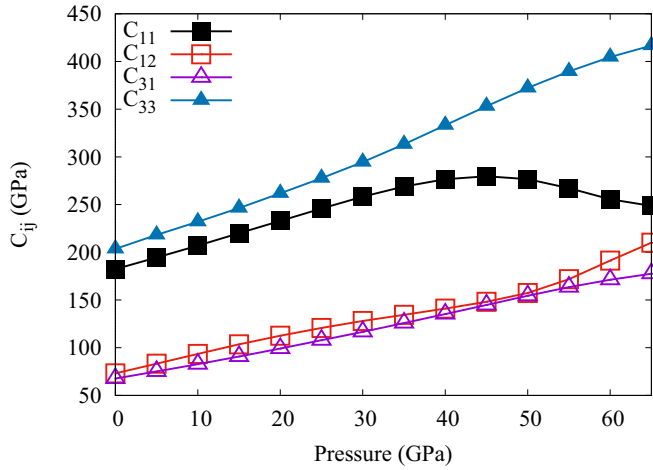


FIG. 9. The dependence of the elastic tensor components  $C_{ij}$  on pressure.

experiment of 54 GPa, is close to the value of 55.7 GPa from the ultrasound data [24].

In addition to the condition  $C_{44} > 0$ , which in this case is weakening, there is also one of necessary and sufficient criteria for the elastic stability of the hexagonal crystal system [25]:

$$C_{11} > |C_{12}|. \quad (2)$$

As we can see from Fig. 10, this condition is sharply weakened more than 3 times with increasing pressure above 40 GPa. Such behavior of the considered dependence explicitly indicates the structural instability of the crystal in the corresponding pressure range.

The  $C_{11}$  ( $=C_{22}$ ) elastic constant characterizing a longitudinal compression (Young's modulus) along the  $x$  ( $y$ ) direction

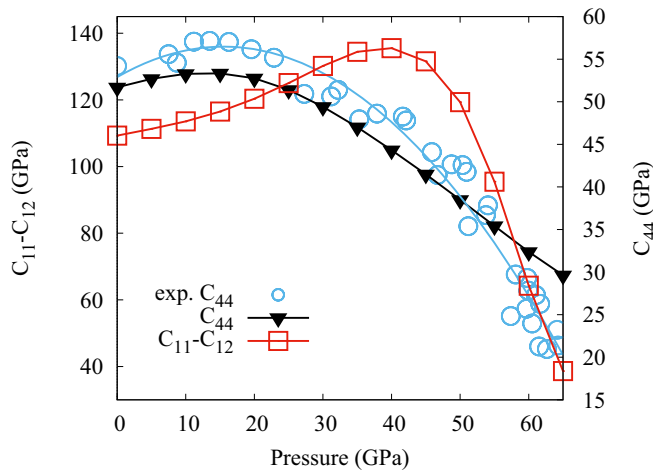


FIG. 10. The dependencies of the elastic tensor component difference  $C_{11} - C_{12}$  and  $C_{44}$  on pressure are denoted by red (left axis) and black curves (right axis) with empty squares and solid triangles, correspondingly. The blue circles and blue curve correspond to the  $C_{44}$  component of the elastic tensor calculated with formula (1) from the experimental data for the frequency of the  $E_{2g}$  phonon mode. The data shown by the blue curve were obtained with the least-squares approximation.

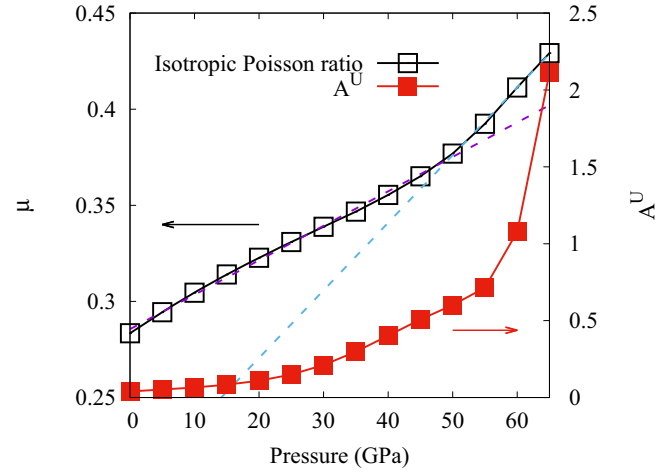


FIG. 11. Isotropic Poisson ratio  $\mu$  and universal anisotropic index  $A^U$ .

has a change in the sign of the derivative in the pressure region of the phase transition. Simultaneously, the behavior of the  $C_{33}$  ( $z$  direction) elastic constant does not undergo similar changes and monotonically increases with increasing pressure. The difference in the dependence of these moduli on pressure indicates a change in the anisotropy of the crystal. The universal elastic anisotropy index  $A^U$  was calculated to verify this assertion by the definition proposed by the authors of [21] in the following form:

$$A^U = 5 \frac{G^V}{G^R} + \frac{K^V}{K^R} - 6, \quad (3)$$

where  $G^V$ ,  $G^R$  and  $K^V$ ,  $K^R$  are the shear and bulk modulus Voigt and Reuss estimates, respectively. The dependence of the universal elastic anisotropy index on the pressure is presented in Fig. 11. As we can see, the value of  $A^U$  monotonically increases with increasing pressure, and it undergoes a jump in the region above 45 GPa, which may indicate a tendency to transition to a more anisotropic phase. Figure 9 also shows the curves of the dependences of the  $C_{12}$  and  $C_{31}$  elastic constants on pressure, which are defined by a transverse extension. As can be seen, the latter has an almost linear dependence on pressure, while the former has an extremum in the region of 45 GPa. This effect is also associated with a slight change in the slope of the Poisson's ratio curve versus pressure at 45 GPa, which can be seen in Fig. 11. Thus, there is a difference between the elastic properties in the  $z$  and  $x, y$  directions. The latter show an anomalous behavior which may serve as a precursor of the structural instability and the phase transition to a more stable phase.

On the basis of the values of the elasticity tensor components, the elastic moduli, the velocities of elastic waves, and the sound velocity were determined in the pressure range from 0 to 65 GPa.

The averaged bulk ( $K_{VRH}$ ) and shear ( $G_{VRH}$ ) moduli were calculated using the Voigt-Reuss-Hill average scheme [26]. The obtained dependencies of  $K_{VRH}$  and  $G_{VRH}$  on pressure are presented in Fig. 12(a). The negative slope of the shear modulus pressure dependence has been found above 40 GPa, which may indicate the shear instability of  $\alpha$ -Hf preceding the

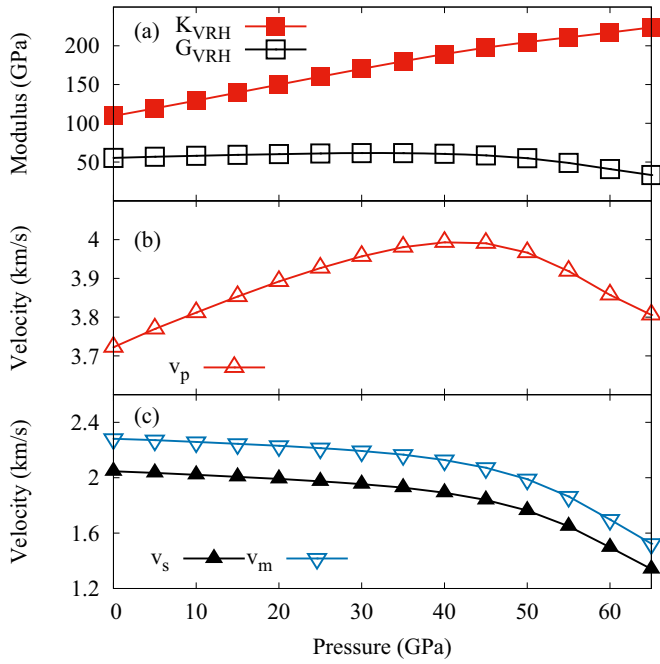


FIG. 12. (a) Adiabatic bulk module  $K$  and shear  $G$  module. (b) Calculated compressional wave  $v_p$  and (c) shear wave  $v_s$  and sound wave  $v_m$  velocities.

transition, as was established for  $\alpha$ -Zr [13]. The average values of the compressional ( $v_p$ ) and shear ( $v_m$ ) wave velocities were evaluated using the formulas [9]

$$v_p = \sqrt{\frac{K_{\text{VRH}} + \frac{4}{3}G_{\text{VRH}}}{\rho}}, \quad v_s = \sqrt{\frac{G_{\text{VRH}}}{\rho}}, \quad (4)$$

where  $\rho$  is the density. The average value of the sound velocity  $v_m$  [9] was calculated as

$$v_m = \left[ 1/3 \left( \frac{2}{v_s^3} + \frac{1}{v_p^3} \right) \right]^{-1/3}. \quad (5)$$

The pressure dependencies of the propagation velocities of elastic waves are shown in Figs. 12(b) and 12(c). The sound and shear wave velocities do not change the sign of the first derivative in the whole considered pressure range, which cannot be said of the compression wave velocity, which has a critical point near 45 GPa, which also corresponds to the critical Poisson's ratio dependence on pressure (Fig. 11) and a sharp weakening of criterion (2) for the elastic stability of the crystal.

To estimate the isotropic Poisson ratio  $\mu$  the following formula was used [27]:

$$\mu = \frac{3K_{\text{VRH}} - 2G_{\text{VRH}}}{6K_{\text{VRH}} + 2G_{\text{VRH}}}. \quad (6)$$

The dependence of  $\mu$  on pressure is shown in Fig. 11 by the solid black curve with open squares.

Figure 11 also has two dashed lines (violet and blue), which were obtained with the least-squares approximation method in two pressure ranges from 0 to 35 GPa and from 50 to 65 GPa, to illustrate the presence of two regions with different slopes of the Poisson's ratio curve versus pressure and the existence of the wide transition region between them.

#### IV. CONCLUSION

In the present study, the Raman scattering experiment under pressure revealed the phonon-softening effect of the  $E_{2g}$  mode corresponding to the oscillations of Hf atoms in the  $xy$  plane. Theoretical calculations of an electronic structure carried out within the framework of the DFT also confirm the presence of this effect. The observed phonon mode softening effect under pressure reflects the close relationship between the electronic and lattice degrees of freedom in  $\alpha$ -Hf. It was found that two effects associated with the charge distribution occur simultaneously with increasing pressure. Growth in the external pressure leads to the rise in the  $5d$  Hf shell occupation due to  $sp-d$  hybridization strengthening. Furthermore, there is a redistribution of the electron density between  $5d$  subshells in favor of subshells corresponding to the orbitals oriented in the  $xy$  plane. The values of the components of the elasticity tensor, the bulk and shear moduli, the isotropic Poisson ratio, and the universal anisotropy index obtained during the calculations demonstrate unusual behavior with increasing pressure that indicates the structural instability of the  $\alpha$  phase and can serve as a good indicator of the appearance of the phase transition. It is known that the temperature of the superconducting transition in hafnium increases substantially under pressure.  $T_c$  is 0.128 K at atmospheric pressure and increases to 8 K at 64 GPa [28]. Anomalous softening of the  $E_{2g}$  mode could be one of the causes of  $T_c$  growth due to a change in the electron-phonon interaction.

#### ACKNOWLEDGMENTS

The present work was supported by a grant of the Russian Science Foundation (Project No. 14-22-00004). The authors thank E. I. Patrakov for electron probe microanalysis of the samples and S. V. Streltsov and Dm. M. Korotin for useful discussions.

[1] H. Xia, G. Parthasarathy, H. Luo, Y. K. Vohra, and A. L. Ruoff, *Phys. Rev. B* **42**, 6736 (1990).  
 [2] R. Hrubiak, V. Drozd, A. Karbasi, and S. K. Saxena, *J. Appl. Phys.* **111**, 112612 (2012).  
 [3] K. K. Pandey, J. Gyanchandani, M. Somayazulu, G. K. Dey, S. M. Sharma, and S. K. Sikka, *J. Appl. Phys.* **115**, 233513 (2014).

[4] J. S. Gyanchandani, S. C. Gupta, S. K. Sikka, and R. Chidambaram, *J. Phys.: Condens. Matter* **2**, 301 (1990).  
 [5] R. Ahuja, J. M. Wills, B. Johansson, and O. Eriksson, *Phys. Rev. B* **48**, 16269 (1993).  
 [6] S. Ostanin and V. Trubitsin, *Comput. Mater. Sci.* **17**, 174 (2000).  
 [7] G. Jomard, L. Magaud, and A. Pasturel, *Philos. Mag. B* **77**, 67 (1998).

- [8] H. Fang, M. Gu, B. Liu, X. Liu, S. Huang, C. Ni, Z. Li, and R. Wang, *Phys. B (Amsterdam, Neth.)* **406**, 1744 (2011).
- [9] Y. Hao, J. Zhu, L. Zhang, H. Ren, and J. Qu, *Philos. Mag. Lett.* **91**, 61 (2011).
- [10] X. Qi, X. Wang, T. Chen, and B. Li, *J. Appl. Phys.* **119**, 125109 (2016).
- [11] H. Olijnyk and A. P. Jephcoat, *Phys. Rev. B* **56**, 10751 (1997).
- [12] Y. S. Ponosov, S. V. Streltsov, and K. Syassen, *High Pressure Res.* **32**, 138 (2012).
- [13] W. Liu, B. Li, L. Wang, J. Zhang, and Y. Zhao, *J. Appl. Phys.* **104**, 076102 (2008).
- [14] Y. Akahama and H. Kawamura, *J. Appl. Phys.* **100**, 043516 (2006).
- [15] A. F. Goncharov, E. Gregoryanz, V. V. Struzhkin, R. J. Hemley, H. K. Mao, N. Boctor, and E. Huang, *Proc. Int. Sch. Phys. "Enrico Fermi"* **147**, 297 (2002).
- [16] G. Kresse and J. Furthmüller, *Phys. Rev. B* **54**, 11169 (1996).
- [17] P. E. Blöchl, *Phys. Rev. B* **50**, 17953 (1994).
- [18] J. P. Perdew and K. Burke, *Int. J. Quantum Chem.* **57**, 309 (1996).
- [19] F. Birch, *Phys. Rev.* **71**, 809 (1947).
- [20] C. Stassis, D. Arch, O. D. McMasters, and B. N. Harmon, *Phys. Rev. B* **24**, 730 (1981).
- [21] S. I. Ranganathan and M. Ostoja-Starzewski, *Phys. Rev. Lett.* **101**, 055504 (2008).
- [22] M. P. Verma and J. C. Upadhyaya, *J. Phys. F* **1**, 618 (1971).
- [23] H. Olijnyk and A. P. Jephcoat, *Metall. Mater. Trans. A* **33**, 743 (2002).
- [24] E. S. Fisher and C. J. Renken, *Phys. Rev.* **135**, A482 (1964).
- [25] F. Mouhat and F.-X. Coudert, *Phys. Rev. B* **90**, 224104 (2014).
- [26] R. Hill, *Proc. Phys. Soc. London, Sect. A* **65**, 349 (1952).
- [27] M. de Jong, W. Chen, T. Angsten, A. Jain, R. Notestine, A. Gamst, M. Sluiter, C. Krishna Ande, S. van der Zwaag, J. J. Plata, C. Toher, S. Curtarolo, G. Ceder, K. A. Persson, and M. Asta, *Sci. Data* **2**, 150009 (2015).
- [28] I. O. Bashkin, M. V. Nefedova, V. G. Tissen, and E. G. Ponyatovsky, *J. Exp. Theor. Phys. Lett.* **80**, 655 (2004).